Asymmetric spin-transfer torque in single-crystalline Fe/Ag/Fe nanopillars

R. Lehndorff, M. Buchmeier, D. E. Bürgler, A. Kakay, R. Hertel, and C. M. Schneider
Institute of Solid State Research, Electronic Properties (IFF-9) and cni—Center of Nanoelectronic Systems for Information Technology, Research Center Jülich GmbH, D-52425 Jülich, Germany

(Received 23 July 2007; revised manuscript received 17 October 2007; published 21 December 2007)

We investigate current-perpendicular-plane giant magnetoresistance (CPP-GMR) and current-induced magnetization switching in single-crystalline Fe/Ag/Fe nanopillars of 70 nm diameter. The interplay between the in-plane, fourfold magnetocrystalline anisotropy of the Fe(001) layers and the spin-transfer torque (STT) gives rise to a two-step switching behavior, which allows an investigation of the angular dependences of CPP-GMR and spin-transfer torque. Both behave asymmetrically with respect to the perpendicular alignment of the two Fe layer magnetizations as theoretically predicted due to strong spin accumulation at the Fe/Ag(001) interfaces [M. D. Stiles and D. R. Penn, Phys. Rev. B **61**, 3200 (2000)]. The asymmetry parameter determined from the STT data quantitatively agrees with calculated spin-dependent interface resistances, whereas CPP-GMR yields a smaller degree of asymmetry.

DOI: 10.1103/PhysRevB.76.214420 PACS number(s): 75.47.−m, 72.25.Ba, 75.60.Jk

I. INTRODUCTION

Spin-transfer torque (STT) and its possible effects of switching the magnetization or exciting steady-state magnetization precessional motions in nanometer-sized magnetic elements attracted a lot of interest since 1996, when Slonczewski[1] and Berger[2] had first predicted these effects. They have been demonstrated experimentally,[3,4] and the understanding of magnetization dynamics driven by STT has grown very quickly.[5] However, there is still a lack of understanding with respect to the microscopic origin of the STT. In our approach, we decided to use well-characterized, single-crystalline magnetic multilayer systems in order to gain further insight into this issue.

Giant magnetoresistance (GMR) and STT are two characteristic magnetotransport phenomena occurring in layered systems consisting of two ferromagnetic (FM) layers separated by a nonmagnetic (NM) interlayer. The common cause for these effects is the fact that the charge carriers and, thus, the current passing through these layers are spin polarized.[1,2] There are two mechanisms giving rise to a finite spin polarization of the current. The first one is simply the natural spin polarization of the charge carriers in a ferromagnet, caused by the imbalance of spin-up and spin-down density of states at the Fermi level. This "ground state" polarization can be transferred through an interface into a NM metal. As the NM metal is characterized by a spin balance, the spin polarization will decay within the NM metal on a length scale given by the spin flip diffusion length (λ_{sd}) of the NM material, as long as there is no additional channel for spin flip scattering, e.g., interfaces with other materials. The second mechanism that can polarize a current is a more subtle one and involves a gradient of the so-called spin accumulation in the NM material during the current flow.[6] In a simple picture, electrons in a NM material can become polarized, because one type of spins, e.g., spin down, accumulates in front of a FM layer (with respect to the electron flux direction), whereas the other type, e.g., spin up, passes through it. The reason for this behavior are the spin-dependent resistivity of the FM material and potential steps at the interfaces, which can differ for the two types of spins, and thus, yield spin-dependent interface resistances. As a consequence, the spin accumulation decays as soon as the current flow stops.

In a FM/NM/FM structure, both of the above mechanisms in each of the FM layers contribute to the polarization of the current in the NM interlayer.[7] The GMR is then given by the component of the spin polarization of the current in the interlayer, which is parallel to the magnetization of the second layer. The STT results from the transversal component, which is absorbed at the interface of the FM layer. Due to spin momentum conservation, the absorbed spin momentum gives rise to a torque on the magnetization of the second FM layer.

For symmetric systems with magnetic layers of equal thickness, Slonczewski gives the following relations for the dependence of the GMR effect, with the current flowing perpendicular to the plane (CPP-GMR) and the STT L_{STT} on the angle ϑ between the two layer magnetizations:[8]

$$r(\vartheta) = \frac{R(\vartheta) - R(0^\circ)}{R(180^\circ) - R(0^\circ)} = \frac{1 - \cos^2(\vartheta/2)}{1 + \chi \cos^2(\vartheta/2)}, \tag{1}$$

$$L_{STT}(\vartheta) = \frac{\hbar I P \Lambda}{4Ae} \frac{\sin(\vartheta)}{\Lambda \cos^2(\vartheta/2) + \Lambda^{-1} \sin^2(\vartheta/2)}, \tag{2}$$

with

$$\Lambda^2 = \chi + 1 = AG\frac{R^+ + R^-}{2}. \tag{3}$$

$R(\vartheta)$ is the dependence of the resistance on ϑ, $G = e^2 k_f^2 / \sqrt{3}\pi h$ the conductance of the interlayer, A the cross sectional area of the nanopillar, $R^{+(-)}$ the total (interface and bulk) resistance for spin-up (spin-down) electrons for one side of the system, and $P = (R^- - R^+)/(R^- + R^+)$ is the spin polarization. The parameters χ and Λ are measures for the deviation from the symmetric behavior, which is given by $\Lambda = 1$ ($\chi = 0$). A system with different layer thicknesses can be described by these equations if the main contributions to the resistances $R^{+(-)}$ arise from the interfaces.[9] Λ^2 expresses the ratio of the mean resistance of one magnetic layer (including

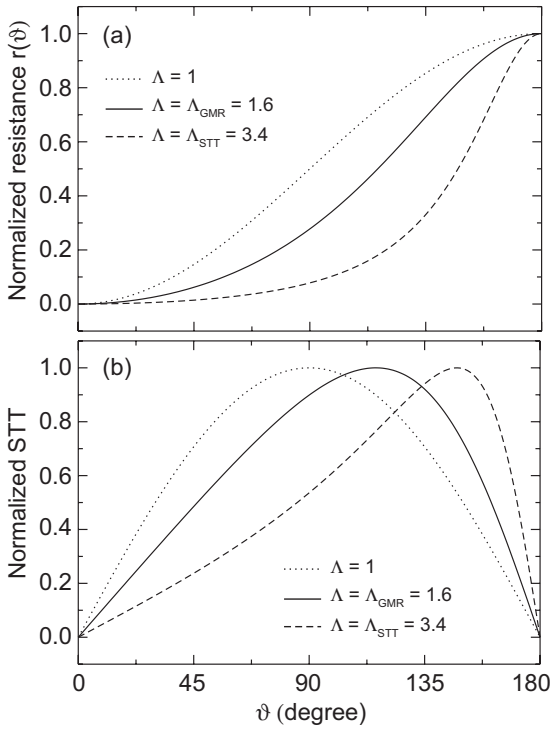

FIG. 1. Angular variations of (a) the GMR signal and (b) the spin-transfer torque for three different Λ (χ) values according to Eqs. (1)–(3). The dotted line shows the symmetric behavior as found experimentally in Ref. 12. The solid line is what we got from our GMR data and the broken line is obtained from our ratio of switching current densities ρ_{c2}/ρ_{c1} (see Table I). The experiment clearly finds a pronounced deviation from the symmetric behavior, which stems from the enhanced spin accumulation at the Fe/Ag(100) interfaces.

the lead) to the intrinsic interlayer resistance. If it deviates from unity, the averaged spin-dependent resistance is different from the interlayer resistance, which leads to an enhanced spin accumulation. For a more detailed description, see Refs. 6, 10, and 11, and references therein.

In Fig. 1, we plot the variations of the GMR and STT signals with the angle ϑ between the magnetization directions of the two FM layers for various values of Λ (χ). The dotted lines for $\Lambda=1$ ($\chi=0$) represent the symmetric case. The GMR ratio is then given by $r(\vartheta)=\sin^2(\vartheta/2)$ with point symmetry about the value at $\vartheta=90°$ as known for current-in-plane GMR. The angular dependence of the STT is reduced to $L_{STT}(\vartheta)\propto\sin(\vartheta)$ and is, thus, mirror symmetric about $\vartheta=90°$. Having $\Lambda\neq1$ breaks this mirror symmetry. Systematic studies on the angular dependence of CPP-GMR in Permalloy/Cu/Permalloy microstructures[13] revealed a behavior given by Eq. (1), with χ ranging between 0.5 and 7 (Λ between 1.2 and 2.8) for different free-layer thicknesses. Thus, the STT should behave as described by Eq. (2). In Ref. 12, the angular dependences of GMR and STT were studied for sputtered CoFe/Cu/Co nanopillars. In these experiments, $\Lambda=1$ was adequate to explain the experimental results. This might be a result of the chosen materials and layer thicknesses. In most cases, an asymmetric behavior of the STT should be expected, but has so far never been observed.

We exploit the interplay between the magnetocrystalline anisotropy of single-crystalline Fe layers and the external field in order to measure the angular dependence of the GMR as well as that of the STT in our system within certain limits. The anisotropy in single-crystalline Fe can be described by the anisotropy energy density[14]

$$E=K_1(m_x^2m_y^2+m_x^2m_z^2+m_y^2m_z^2), \tag{4}$$

where K_1 is the magnetocrystalline anisotropy constant and $m_{x,y,z}$ are the components of the reduced magnetization. The shape anisotropy forces the magnetization of our Fe films into the plane of the sample, where the magnetocrystalline anisotropy gives rise to a fourfold symmetry with the easy axes along Fe(100)[100] directions. In contrast, the angular dependence of the STT is twofold [see Fig. 1(b)] as is the in-plane shape anisotropy of the elliptical samples usually used by others.

II. SAMPLE PREPARATION AND FABRICATION

A layer stack of 1 nm Fe, 150 nm Ag, 20 nm Fe (fixed layer), 6 nm Ag (interlayer), 2 nm Fe (free layer), and 50 nm Au is grown by molecular beam epitaxy onto an annealed GaAs(100) substrate. Low energy electron diffraction is used to ensure that all layers are single crystalline and epitaxial. Patterning starts with optical lithography to define the bottom electrodes, which are then formed by ion beam etching (IBE). Using hydrogen silsesquioxane (HSQ) as electron beam resist, we define the circular nanopillars, which have a diameter of 60 nm after developing. IBE under changing incident angle while rotating the sample leads to structure diameters of 70 nm. Etching is timed such that only the top 2-nm-thick Fe free layer is structured, but the 20-nm-thick fixed layer underneath is not. The sample is then spin coated with a layer of HSQ to planarize the surface. Subsequently, 50 nm of silicon nitride are deposited by plasma enhanced chemical vapor deposition as an additional insulating layer. Then, a 10×10 μm^2 window above the nanopillar is defined by optical lithography, within which the insulating layers are removed by IBE and reactive ion etching with trifluoromethane. Finally, the top electrode is defined by optical lithography, and a bilayer of 5 nm Ti and 200 nm Au is evaporated onto the sample and structured using lift-off technique. The preparation and fabrication procedures are described in more detail in Ref. 15.

III. EXPERIMENTAL RESULTS

All measurements are performed inside a cryostat at a temperature of 5 K to ensure that the magnetic behavior is not dominated by thermal excitations. A magnetic field of up to 1.2 T can be applied in the plane of the sample. Rotation of the sample about the surface normal allows one to align the field along any in-plane direction.

A. Giant magnetoresistance

First, we measure the CPP-GMR effect in a four-point geometry. We apply a direct current of 1 mA, which is below

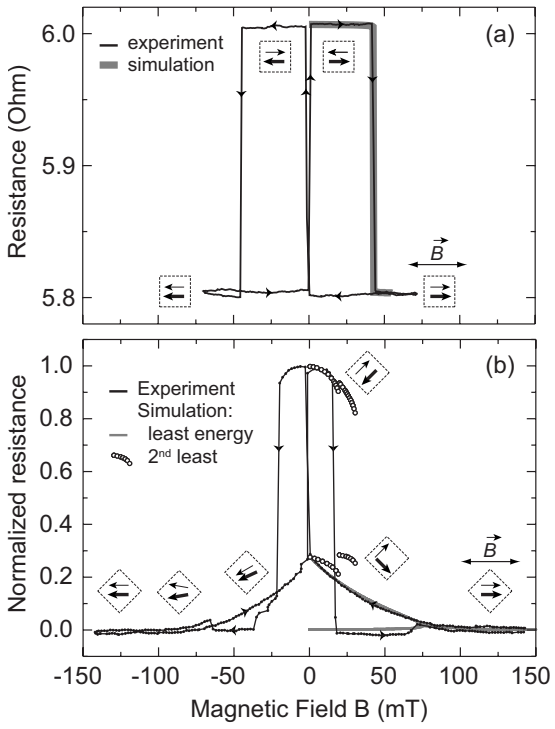

FIG. 2. CPP-GMR data (black) measured at 5 K with the magnetic field being applied along (a) an easy or (b) hard axis, respectively, of the single-crystalline Fe layers. Gray lines are least and circles are second least energy solutions of Stoner-Wohlfarth fits. Equation (1) is used to calculate the GMR signal. The fit parameters are $\chi_{GMR}=1.6$ ($\Lambda_{GMR}=1.6$), $K_1^{free}=63$ kJ/m^3, and $K_1^{fixed}=98$ kJ/m^3. The edges of the dashed squares indicate the magnetic easy axis of the Fe layers and the thick (thin) arrow indicates the magnetization direction of the fixed (free) layer.

the critical value for current-induced magnetic excitations or switching. Figures 2(a) and 2(b) show major GMR loops of the same contact for the field applied along magnetic easy (EA) and hard axes (HA) of the Fe layers, respectively. The curves reveal very different switching behavior. The measurements start from positive saturation of the system. For the first case, ($B\|$EA), the resistance remains basically constant for decreasing positive field. At a very small negative field of about −2 mT, the extended 20 nm Fe layer reverses its magnetization direction so that the relative alignment to the magnetization of the 2-nm-thick Fe nanodisk reaches $\vartheta=180°$, resulting in a highly resistive state that is stable down to −40 mT. At this field value, the nanodisk switches its magnetization direction to align with the field direction and, thus, parallel to the fixed Fe layer. The result is a low-resistive state again. The behavior is symmetric when the magnetic field is swept from negative to positive values. The maximum GMR value amounts to 3.3%.

For the second case, ($B\|$HA), the resistance increases smoothly from about 90 to 0 mT. In this region, the two magnetization vectors rotate in opposite directions away from the hard axis toward two different easy axes. This results in a relative angle of $\vartheta=90°$ at 0 mT according to the fourfold crystalline anisotropy of the Fe layers. Then, at about −2 mT, the extended 20 nm Fe layer switches to an antiparallel orientation with respect to the magnetization of the 2 nm Fe nanodisk. Therefore, the state with highest resistivity is reached. With increasing magnitude of the negative field, the two magnetizations are drawn from the EA toward the field direction. This shows up in the rounding off at the top of the magnetoresistance curve. At −20 mT, the magnetization of the nanodisk switches into a parallel orientation to the magnetization of the 20 nm Fe layer. However, in both layers, the magnetization is not yet saturated in the HA direction, as can be seen from a further resistance increase at −60 mT. At this point, one of the two magnetizations switches from an orientation slightly left of the HA to an energetically identical orientation slightly right of this axis. Then, with decreasing field, both magnetization vectors are pulled further toward the HA until saturation is reached at −90 mT. Again, the behavior is identical for the reversed sweep direction.

A large qualitative difference can be seen in the switching behavior of the two magnetic layers. The part of the thicker, but extended layer that is probed in these measurements (i.e., the part below the nanodisk) reverses at very low fields, since only domain wall nucleation and movement are needed in this process. The nanodisk shows switching fields that are significantly higher, indicating that it is well in the single-domain regime, where no domain walls can be created inside the disk. The applied field has to overcome the energy barrier given by the magnetocrystalline anisotropy for the whole nanodisk at once.

For further analysis, we performed micromagnetic simulations of a circular disk with a diameter of 70 nm and a thickness of 2 nm using an algorithm based on the finite element method combined with the boundary element technique.[16,17] The switching fields assigned to the nanodisk in the experiment are very well reproduced by the simulations when an anisotropy energy constant K_1^{free} of 60 kJ/m^3 and a saturation magnetization M_S of 1.6 MA/m are used. The literature value of K_1 for bulk Fe at room temperature is 52 kJ/m^3. Strictly speaking, we can only extract the ratio K_1/M_S from switching or saturation fields. Therefore, there is an uncertainty in the determination of K_1^{free}, because an Fe layer of only 2 nm thickness could show a reduced M_S as compared to the bulk. In any case, the good agreement with the experimental data indicates single-domain behavior and justifies the application of the Stoner-Wohlfarth model.

A very interesting magnetic configuration can be inferred from the GMR measurements with the magnetic field applied parallel to a HA [Fig. 2(b)]. The two magnetizations rest in two different EA when the field is decreased to zero and will, thus, include an angle of 90°. For a standard angular dependence of the GMR, $r(\vartheta)=\sin^2(\vartheta/2)$, $r(90°)$ would be 0.5. Instead, in Fig. 2(b), we find a much lower value of 0.3. This deviation originates from spin accumulation at the FM/NM interfaces, and is a clear indication of the strength of this mechanism in our samples. In order to describe this finding in a more quantitative manner, we fit the data in Fig. 2(b) using the Stoner-Wohlfarth model including Zeeman energy and cubic anisotropy, and calculate local energy minima for the relative alignment of the magnetizations with respect to the external field.[14] The corresponding values of $r(\vartheta)$ are obtained from the enclosed angle ϑ and Eq. (1). Fitting pa-

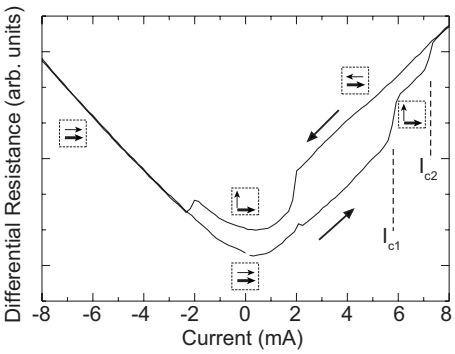

FIG. 3. Two-step current-induced switching of the free-layer magnetization at 5 K. A weak field of 5.6 mT is applied along a HA. I_{c1} and I_{c2} denote the critical currents for the switching from parallel to perpendicular alignment and from perpendicular to antiparallel alignment, respectively.

rameters are the magnetocrystalline anisotropy constants of the free and fixed layers, K_1^{free} and K_1^{fixed}, the resistance levels for parallel and antiparallel alignments of the magnetizations, $R(0°)$ and $R(180°)$, and, most interestingly, the parameter χ. In Fig. 2(b), the two energetically most favorable states are plotted as gray lines and circles. They match the measured data very well and confirm again the single-domain behavior of the nanodisk. The extracted parameters are $\chi_{GMR}=1.6\pm0.1$ ($\Lambda_{GMR}=1.6\pm0.03$), $K_1^{free}=63$ kJ/m^3, and $K_1^{fixed}=98$ kJ/m^3.

B. Spin-transfer torque

In the next step, we measure the differential resistance versus dc current to examine the current-induced magnetization switching. Figure 3 shows a dc current loop taken at an applied magnetic field of 5.6 mT parallel to a HA. The measurement starts in a low-resistive state at zero dc current. This state was prepared by a previous current sweep that started with an antiparallel alignment of free-layer and fixed-layer magnetizations, as the low-resistive state at 5.6 mT cannot be prepared by a field sweep. Two switching processes can be distinguished upon increasing the current. The first at +5.8 mA leads to an intermediate resistive state, the second at +7.3 mA to a highly resistive state. When the current decreases again, the system falls back to the intermediate resistive level at +1.9 mA. At −2.1 mA, the free-layer magnetization is switched into a parallel alignment to the fixed layer and the low-resistive level is reestablished. The intermediate resistive level is assigned to a perpendicular alignment of the two magnetizations due to the crystalline anisotropy. Obviously, the magnetization switches in two steps from the parallel to the antiparallel alignment via an intermediate 90° state. In the following, I_{c1} (I_{c2}) denotes the critical current for switching from 0° to 90° (90° to 180°).

The behavior in Fig. 3 is representative of magnetic fields of nearly any orientation, but with a magnitude well below the coercive field of the free layer. Under these conditions, the anisotropy dominates the switching process. Thus, the two-step switching process with two different critical currents results from the interplay between the magnetocrystalline anisotropy and the spin-transfer torque. The applied magnetic field stabilizes the fixed layer in a certain direction and imposes on the free magnetization a preferred rotational direction for switching.

The first critical current value I_{c1} is reached when the STT overcomes the damping, which is proportional to the effective field $H_{eff}=-dE/dM$. In our case, the anisotropy is the dominant contribution to H_{eff}. The second critical current I_{c2} is determined by the asymmetry of the STT with respect to the $\vartheta=90°$ alignment. As confirmed by simulations for this starting condition, the magnetization of the free layer starts a small-angle precession around the easy axis at $\vartheta=90°$ driven by the dc current. In this geometry, however, the precession is damped by the STT for one part of the precession trajectory with $\vartheta<90°$, because then STT and damping are parallel and point towards the easy axis. For other parts of the trajectory with $\vartheta>90°$, the two contributions oppose each other and the STT acts as an excitation. An asymmetry of the STT favors excitation over damping. The stronger the asymmetry, the lower the I_{c2}. In the symmetric case ($\Lambda=1$), I_{c2} becomes very large because the damping and exciting torques along the precession trajectory largely compensate each other.

In Table I, we compile the experimental data for contact A

TABLE I. Compilation of parameters derived from the experiments and simulations for two contacts A and B. The anisotropy constants K_1^{free} and K_1^{fixed} as well as $r(90°)$ are determined from GMR curves (e.g., Fig. 2). Λ_{GMR} is calculated from $r(90°)$ using Eqs. (1) and (3). Critical current densities ρ_{c1} and ρ_{c2} are obtained by dividing $I_{c1,c2}$ (e.g., Fig. 3) by the contact cross section $A=3.85\times10^{-15}$ m^2. For the simulations, we use a constant K_1^{free} and vary Λ_{STT} to obtain $r(90°)$ and the ratio ρ_{c2}/ρ_{c1}. For $\Lambda_{STT}=1.6$, we match the experimental $r(90°)$ but not ρ_{c2}/ρ_{c1} and vice versa for $\Lambda_{STT}=3.4$.

	GMR data				STT data		
Contact	K_1^{free} (kJ/m^3)	K_1^{fixed} (kJ/m^3)	$r(90°)$	Λ_{GMR}	ρ_{c1} (10^{11} A/m^2)	ρ_{c2} (10^{11} A/m^2)	ρ_{c2}/ρ_{c1}
A	63	98	0.3	1.6	15.1	19.0	1.26
B			0.2	1.7	19.2	24.4	1.27
Simulation $\Lambda_{STT}=1.6$	60		0.3		16.0	46.0	2.88
Simulation $\Lambda_{STT}=3.4$	60		0.08		15.7	19.7	1.25

discussed in detail in Figs. 2 and 3 together with data from a second nanopillar (contact B) on the same sample, and compare them with the results of the simulations. The magnetocrystalline anisotropy constants K_1 are derived from fitting the switching fields in the CPP-GMR measurements. The reduced resistance in the perpendicular state, $r(90°)$, allows the determination of Λ_{GMR} using Eqs. (1) and (3). From the resistance versus dc current measurements at low magnetic fields, we extract $I_{c1,c2}$ and the critical current densities $\rho_{c1,c2}=I_{c1,c2}/A$, and obtain the ratio ρ_{c2}/ρ_{c1}. This ratio is the most relevant parameter for the comparison of experiment and simulation, since it excludes uncertainties in nanopillar size, anisotropy constant, damping parameter α, or polarization degree of the dc current P. The latter two are chosen parameters for the following simulations.

IV. SIMULATIONS

For the macrospin simulations of current-induced magnetization switching, we use the expression for the spin-transfer torque given by Eq. (2) with appropriate prefactors according to Ref. 8. First, we use $\Lambda_{STT}=\Lambda_{GMR}=1.6$ as determined experimentally for contact A from $r(90°)$. Further parameters for the macrospin simulations are the damping parameter $\alpha=0.01$, current polarization $P=0.3$, and a magnetic field of 2.6 mT, which is applied parallel to a HA. The resulting values for the critical current densities are $\rho_{c1}=16.0\times10^{11}$ A/m^2 and $\rho_{c2}=46.0\times10^{11}$ A/m^2, yielding $\rho_{c2}/\rho_{c1}=2.88$ (second to last line in Table I). This value is more than twice the experimental results for contacts A and B. Increasing the input Λ_{STT} to 3.4 yields a ratio $\rho_{c2}/\rho_{c1}=1.25$, close to the experimental value of both contacts (last line in Table I).

If we calculate Λ by Eq. (3) using the values $A=3.85\times10^{-15}$ m^2, $G_{\mathrm{Ag}}=1.16\times10^{15}$ Ω^{-1} m^{-2} (using k_F from Ref. 18), and spin-dependent interface area resistances of $AR^{+}_{\mathrm{Fe/Ag(100)}}=1.07\times10^{-15}$ Ω m^2 and $AR^{-}_{\mathrm{Fe/Ag(100)}}=12.86\times10^{-15}$ Ω m^2 as calculated by Stiles and Penn,[19] we get $\Lambda=4$. We thereby neglect bulk resistance contributions [52 $\mu\Omega$ for the thicker Fe layer using $\rho^{\mathrm{Fe}}=1.0\times10^{-11}$ Ω m at 10 K (Ref. 20)] since they are 3 orders of magnitude smaller than the interface resistances $R^{+}_{\mathrm{Fe/Ag(100)}}=0.28$ Ω and $R^{-}_{\mathrm{Fe/Ag(100)}}=3.3$ Ω. This calculated value of $\Lambda=4$ agrees well with our result $\Lambda_{STT}=3.4$ determined from simulations that match the experimentally observed ratios ρ_{c2}/ρ_{c1} (last line in Table I).

V. DISCUSSION

In both the GMR and STT results, we find a strong influence of the spin accumulation, leading to an asymmetric angular variation of these quantities. While the asymmetry parameter $\Lambda_{STT}=3.4$ ($\chi_{STT}=10.6$) of the STT fits well to calculated spin-dependent interface resistances, the asymmetry of the GMR $\Lambda_{GMR}=1.6$ ($\chi_{GMR}=1.6$) is found to be much smaller.

One possible reason for this deviation from the theoretical predictions is that we neglect any coupling between the two layers in our nanopillars, since there is no corresponding evidence in the static GMR measurements. There could still be a finite, possibly dynamic interaction of the stray field of the structured free layer with the unstructured fixed layer. Oxidation of the edges of the free layer and the surface of the fixed layer could introduce pinning, which might explain the large anisotropy constants. All these effects could also be a reason for the different degrees of asymmetries that we derive for the CPP-GMR and STT behaviors.

VI. CONCLUSION

We measured the angular variations of CPP-GMR and the critical current density for current-induced magnetization switching in single-crystalline Fe/Ag/Fe nanopillars by exploiting the interplay between the magnetocrystalline anisotropy of Fe and the STT. Both dependences show a significant deviation from the symmetric form. This feature has been predicted by theory,[8] but has not been observed so far. It originates from strong spin accumulation at the Fe/Ag(100) interfaces. Our analysis shows that these spin accumulation effects can be understood on a quantitative basis by means of micromagnetic calculations.

ACKNOWLEDGMENTS

We would like to thank P. Grünberg for valuable discussions and F.-J. Köhne for technical support.

[1] J. C. Slonczewski, J. Magn. Magn. Mater. **159**, L1 (1996).
[2] L. Berger, Phys. Rev. B **54**, 9353 (1996).
[3] J. A. Katine, F. J. Albert, R. A. Buhrman, E. B. Myers, and D. C. Ralph, Phys. Rev. Lett. **84**, 3149 (2000).
[4] S. I. Kiselev, J. C. Sankey, I. N. Krivorotov, N. E. Emley, R. J. Schoelkopf, R. A. Buhrman, and D. C. Ralph, Nature (London) **425**, 380 (2003).
[5] M. D. Stiles and J. Miltat, *Spin Dynamics in Confined Magnetic Structures III* (Springer, Berlin, 2006).
[6] M. D. Stiles and A. Zangwill, Phys. Rev. B **66**, 014407 (2002).
[7] M. D. Stiles and A. Zangwill, J. Appl. Phys. **91**, 6812 (2002).
[8] J. C. Slonczewski, J. Magn. Magn. Mater. **247**, 324 (2002).
[9] J. Xiao, A. Zangwill, and M. D. Stiles, Phys. Rev. B **70**, 172405 (2004).
[10] A. A. Kovalev, A. Brataas, and G. E. W. Bauer, Phys. Rev. B **66**, 224424 (2002).
[11] J. Barnas, A. Fert, M. Gmitra, I. Weymann, and V. K. Dugaev, Phys. Rev. B **72**, 024426 (2005).
[12] F. B. Mancoff, R. W. Dave, N. D. Rizzo, T. C. Eschrich, B. N. Engel, and S. Tehrani, Appl. Phys. Lett. **83**, 1596 (2003).
[13] S. Urazhdin, R. Loloee, and W. P. Pratt, Jr., Phys. Rev. B **71**, 100401(R) (2005).
[14] M. Buchmeier, B. K. Kuanr, R. R. Gareev, D. E. Bürgler, and P. Grünberg, Phys. Rev. B **67**, 184404 (2003).

[15] H. Dassow, R. Lehndorff, D. E. Bürgler, M. Buchmeier, P. A. Grünberg, C. M. Schneider, and A. van der Hart, Appl. Phys. Lett. **89**, 222511 (2006).
[16] R. Hertel, J. Appl. Phys. **90**, 5752 (2001).
[17] R. Hertel, W. Wulfhekel, and J. Kirschner, Phys. Rev. Lett. **93**, 257202 (2004).
[18] J. J. Paggel, T. Miller, and T.-C. Chiang, Phys. Rev. Lett. **83**, 1415 (1999).
[19] M. D. Stiles and D. R. Penn, Phys. Rev. B **61**, 3200 (2000).
[20] J. Bass and K. H. Fischer, *Metals: Electronic Transport Phenomena: Electrical Resistivity, Kondo and Spin Fluctuation Systems, Spin Glasses and Thermopower*, edited by K.-H. Hellwege and J. L. Olsen, Landolt-Börnstein, New Series, Group III, Vol. 15, Pt. A (Springer, Berlin, 1982), p. 36.